energies

MDPI

Article

Phase Change Materials (PCMs) Based in Paraffin/Synthetic Saponite Used as Heat Storage Composites

Raquel Trujillano *, Beatriz González and Vicente Rives *

GIR-QUESCAT, Departamento de Química Inorgánica, Universidad de Salamanca, 37008 Salamanca, Spain; bei@usal.es

* Correspondence: rakel@usal.es (R.T.); vrives@usal.es (V.R.)

Abstract: Synthetic saponites were successfully used to prepare phase change materials (PCMs) based on paraffin/synthetic saponite. Paraffin/synthetic saponites PCMs were prepared by a solution intercalation process. The PCMs were characterized by powder X-ray diffraction, FT-IR spectroscopy, thermal analyses and nitrogen adsorption. The thermal properties and the stability of PCMs were measured by DSC analysis and from heating–cooling curves. The results showed that the prepared PCMs have a higher heating rate and a lower cooling speed than paraffin because the heat storage was improved with the synthetic saponite. A one-pot synthesis method for obtaining PCM has been successfully developed in this work. The material thus obtained had better results for heat storage applications.

Keywords: clay; one-pot synthetic organophilic saponite; phase change materials

Citation: Trujillano, R.; González, B.; Rives, V. Phase Change Materials (PCMs) Based in Paraffin/Synthetic Saponite Used as Heat Storage Composites. *Energies* **2021**, *14*, 7414. https://doi.org/10.3390/en14217414

Academic Editors: Simona Bennici and Mohamed Zbair

Received: 30 September 2021
Accepted: 5 November 2021
Published: 8 November 2021

1. Introduction

The use of paraffin as a phase change material has many advantages, e.g., low cost, high energy storage density (amount of energy stored per mass unit), chemical stability, small changes in volume during the phase change process, etc. [1]. However, leakage while in the molten state and its low thermal conductivity [2], as well as its flow ability during the phase change process, make it necessary to develop composite PCMs in order to fix and stabilize the PCMs in structures [3]. Clay minerals have been widely used for the preparation of PCMs, due to their low price and high thermal stability. Among the clays used to prepare these composites, saponite, kaolin, diatomite, sepiolite, perlite and vermiculite are of note [4–6].

Clays' properties make them suitable for use as industrial raw materials in the construction, agricultural, textile, paper, pharmaceutical, ceramic, electrical, nuclear energy, and petroleum industries [7].

Their main advantages are that they are broadly distributed on the Earth's surface and their low cost; their synthesis is also easy and cheap in most cases. In addition, they play an important role in environmental protection, being able to be used as an adsorbent of polluting gases, heavy metals, dyes, and biocides or antibiotics from water, as well as cleaning agents in aquatic systems [8]. Among the different clays, specifically smectite-type clays, bentonites are used as fillers in composites to enhance the properties of the polymeric matrix. In this field, Toyota's work was pioneering in the study of the exfoliation of clay in nylon-6 [9–11], and this work made important progress in the study of the engineering properties of smectites [12–14].

Recently, a great number of studies have been carried out in order to investigate the use of clays as a thermal energy storage medium, since they are able to undergo reversible hydration/dehydration processes [5–16]. As can be seen in the literature, special attention has been focused on phase change materials (PCMs) as latent heat storage systems [4–17] and materials with good absorption properties, such as bentonite [14], that are able to store heat in a latent form.

Cárdenas-Ramírez et al. [18] have recently reported a survey on different materials used for the encapsulation and shape stabilization of PCMs. Clays play an important role as supporting materials used for shape stabilization of organic PCMs [19]. Clay mineral-based materials have exceptional porosity and a high specific surface area. Thus, they can easily harbor the PCMs and offer remarkable shape stabilization. They also have the advantage of substantial reserves and moderate cost [20].

Sari et al. [6] and Li et al. [21] investigated the thermal performances of paraffin/bentonite composite PCMs, reporting that the heat transfer rate of paraffin/bentonite composites was larger than that of paraffin only, demonstrating the beneficial role of bentonite in the composite. These interesting properties of bentonites arise from their structure, formed by sheets of $[SiO_4]^{4-}$ tetrahedra connected to layers of octahedra holding either Al^{3+} (montmorillonite) or Mg^{2+} (saponite) in their centers [22].

Despite their, as mentioned above, easy accessibility and low cost, natural clays need to be modified before their use in specific applications to optimize their behaviour via different techniques that require high temperatures, acid or basic activation treatments, intercalating agents or hydrothermal treatments [10]. The aim of this work is to present new results which avoid unnecessary energy waste and the use of reagents whose elimination contaminates the water and the atmosphere. In this study we have investigated a preparation of a PCM composite of paraffin using synthetic saponite as a support. The saponite used has been synthesized through a fast, efficient, low cost, and environmentally friendly method developed in our laboratory in order to obtain customized saponites [1]. Three types of saponites have been tested; the first was a synthetic saponite used "as synthesized" as a direct carrier of the paraffin, while the other two were organophillized via two different methods in order to compare their structural and thermal properties. The characterization was achieved from their powder X-ray diffractograms, FT-IR spectra, thermal analysis (TG and DTA) and specific surface area measurements. The thermal properties of the PCM composites prepared were determined by temperature distribution curves during heating/cooling processes and by DSC. A one-pot synthesis method for obtaining PCM has been successfully developed in this work. The material thus obtained showed better results for heat storage applications.

2. Materials and Methods

2.1. Synthesis Procedure

To obtain parent saponite, a method described in the literature [23] was followed; briefly, 10 mL of an aqueous solution (A) containing 10.1 mmol of $AlCl_3 \cdot 6H_2O$ and 61.28 mmol of $MgCl_2$ was added to another aqueous solution (B) prepared by adding 11.2 mL of a sodium silicate solution (1.39 g/cc Aldrich) to 100 mL of an aqueous solution of 7.22 g of NaOH and 13.14 g of $NaHCO_3$. Chemicals, except for sodium silicate (supplied by Aldrich), were from Panreac. The pH of solution B was around 13.

Solution A was dropwise added to solution B under constant magnetic stirring; once the addition was complete, the white gel obtained was sealed in a 100 mL Teflon reactor and hydrothermally treated in a Milestone Ethos Plus microwave furnace at 180 °C for 2 h. Then, the solid was washed with distilled water by centrifugation to remove chloride anions and dried overnight at 100 °C. The final solid thus obtained was labelled as S.

Solid S was intercalated with cetyl trimethyl ammonium (CTAB) following the method reported by Li et al. [21]; 85 mL of an aqueous solution containing 1.6 g of CTAB was added to a suspension of 4 g of S in 400 mL of water. The pH of the suspension was adjusted to 6 using concentrated HCl. The resulting mixture was maintained for 3 h in a water bath at 75 °C. After the reaction had finished, the suspension was filtered and washed with water and finally dried in an oven at 70 °C; the sample thus obtained was labelled as SC.

To directly obtain a CTAB intercalated synthetic saponite, 1.6 g of CTAB was added to the initial solution (A + B + CTAB), the mixture was sealed into a 100 mL Teflon reactor and hydrothermally treated in a Milestone Ethos Plus microwave furnace at 180 °C for 2 h, and then washed and dried. The sample thus obtained was labelled as CS.

The intercalation of paraffin was carried out following a method described in the literature [21]. Four grams of the corresponding saponite (S, SC or CS) was suspended in 200 mL of ethanol. Meanwhile, 8 g of paraffin were dissolved in 200 mL of ethanol and added to the clay suspension at room temperature. The resulting mixture was maintained for 5 min under constant stirring. Then, the suspension was placed in a rotary evaporator at 75 °C until the alcohol was evaporated. Finally, the product was dried in a vacuum oven at 80 °C for 24 h. The final nanocomposites were labelled as SP, SCP and CSP.

2.2. Characterization

Element chemical analyses were carried out at Servicio General de Análisis Químico Aplicado (Universidad de Salamanca), using inductively coupled plasma–atomic emission spectrometry (ICP–AES). Samples were digested in HNO_3/HF under microwave irradiation for elemental chemical analysis.

The powder X-ray diffraction (PXRD) patterns of the samples were recorded between 2 and 65° (2θ) at a scanning speed of 2°/min, using a Siemens D-500 diffractometer, operating at 40 kV and 30 mA, and using Ni-filtered Cu Kα radiation (λ = 1.5418 Å). The FT-IR spectra were recorded in the 4000–450 cm^{-1} range in a PerkinElmer Spectrum-One spectrometer using the KBr pellet method. Thermal analyses (TG, DTA and DSC) were performed on an SDT Q600 TA instrument, under a flow of 20 mL/min of oxygen (L'Air Liquide, Spain, 99.999%) and a heating rate of 10 °C/min up to 1000 °C for TG and DTA analysis and 5 °C/min for DSC. The differential thermogravimetric curves (DTG) were calculated from the TG curves using the software controlling the thermal analysis equipment. The textural properties were determined from nitrogen (L'Air Liquide, 99.999%) adsorption–desorption isotherms at −196 °C, using a Micrometrics Gemini VII 2390 t surface area and porosity apparatus. The specific surface area (SSA) was calculated using the BET method, the external surface area and micropore volume by means of the t-method, and the total pore volume from the amount of nitrogen adsorbed at a relative pressure of 0.95 [24–26].

The heat storage and release ability of the samples were determined following the protocol established by Li et al. [27]. The samples were placed in a 10 mL glass tube that was heated at 70 °C in a water bath. Once this temperature was reached, the tube was immediately transferred to a water bath at room temperature (ca. 25 °C). The temperature was measured every 5 s. Once the process concluded, the sample was put back into the bath at 70 °C to study the thermal stability of the PCMs.

3. Results

3.1. Characterization of Saponites and PCMs

The chemical analysis results of the synthesised saponite gave the values of 36.58% of SiO_2, 4.18% of Al_2O_3, 20.74% of MgO and 2.80% of Na_2O. Thus, the rough formula of the synthesised saponite was $[Si_{6.990}\ Al_{0.949}]\ [Mg_{5.990}]\ O_{20}(OH)_4\ [Na_{1.036}]\cdot 22.5H_2O$. The Al^{3+} cations occupied around 0.94 tetrahedral positions, (Si^{4+}+Al^{3+}) occupied 7.94 tetrahedral positions out of the eight possible and Mg^{2+} ions occupied 6.00 octahedral positions out of the six possible. These results confirm the trioctahedral character of the saponite [28,29].

Figure 1 shows the powder X-ray diffractograms (PXRD) of samples S, SC, CS and of the composites SP, SCP and CSP. As can be seen, all the characteristic peaks of natural saponites were recorded, showing that the individual layers were perfectly formed. However, the diffraction expected for the (001) planes was not recorded; most likely this was due to the fact that the sheets were mostly disordered along the *c* axis, without any long-range ordering. Reflection (06.33), due to planes within the sheet, is not dependent on the stacking degree; it is very sensitive to the nature of the cations in the octahedral holes. It has been recorded as 1.48 Å in dioctahedral smectites and as close to 1.53 Å in trioctahedral smectites, such as saponites [28,29]; in our case, it was recorded at 1.53 Å, confirming a trioctahedral structure.

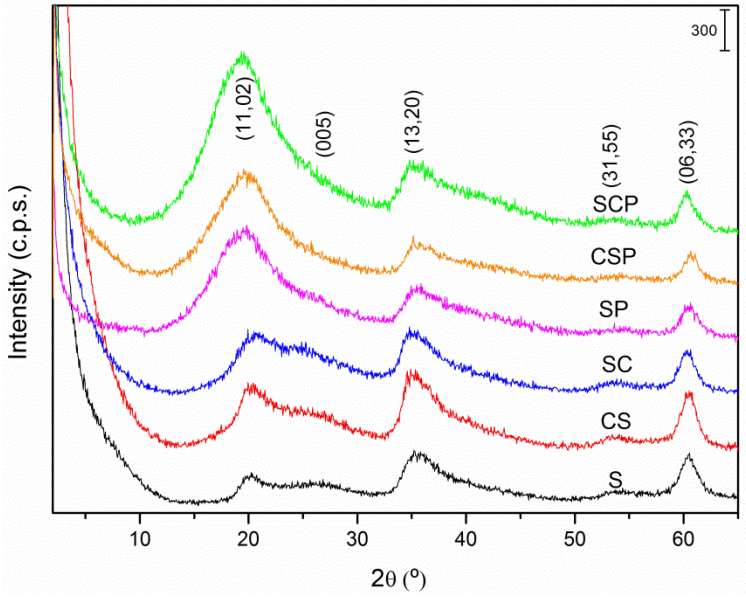

Figure 1. X-ray diffractograms of the saponite (S) the organosaponites (SC and CS) and the PCM nanocomposites.

As can be observed in Figure 1, intercalation with CTAB (Samples SC and CS) did not modify the general shape of the diffraction diagrams (positions and relative intensities of the signals recorded), indicating that intercalation does not give rise to any improvement in the stacking of the layers along direction c. Concerning the diffractograms of the PCM nanocomposites, the peaks recorded are again very similar in all cases and with respect to the starting clays. The (11,02) signal shows a high intensity and thus obscures the peak caused by (005), which is now almost unobservable.

The FT-IR spectra of all samples are shown in Figure 2; the spectrum of the paraffin has been added for comparison. The spectrum of sample S shows the characteristic bands caused by the presence of a saponite: the broad band centered at 3454 cm^{-1} is due to the stretching mode of the O–H groups of the H_2O molecules, and it is extremely broad because of the presence of hydrogen bonds between the water molecules; the band at 1641 cm^{-1} is due to the bending mode of H_2O molecules. The strong, sharp band at 1012 cm^{-1} is due to the vibrations of the Si–O–M–O–Si bonds. In addition, the very weak signal at 814 cm^{-1} can be ascribed to the presence of a small amount of amorphous silica, while the weak band at 656 cm^{-1} corresponds to the vibrational mode of Mg–O bonds in the octahedra [30,31]. The sharp, weak band close to 1380 cm^{-1} is due to nitrate impurities present in the KBr used, and is recorded with different intensities in the spectra of all samples.

The spectra of the samples intercalated with CTAB (SC and CS) show, in addition to the bands described above for the saponite phase without any appreciable change, the characteristic bands of an organic molecule—primarily, the C–H vibrations of an organic chain close to 2958, 2922 and 2853 cm^{-1}. The very weak band recorded at 1470 cm^{-1} can be ascribed to a small amount of carbonate adsorbed on the external surface of the solid particles and to the C–H bending vibration [32].

The FT-IR spectrum of composite SP shows some additional bands to those recorded in the spectrum of sample S; the three bands between 3000 and 2800 cm^{-1} are due to the C–H stretching bonds of its hydrocarbon chain, confirming the presence of paraffin in the composite [33]. The bands at 1464 and 1376 cm^{-1} are due to CH_2 and CH_3 C–H deformation modes, respectively. The band at 722 cm^{-1} is due to the (CH_2) in-phase rocking mode. These bands are recorded in the spectra of all three composites (SP, SCP, and CSP) and they confirm and verify the existence of a number of paraffinic bonds (–CH_2–) in the prepared composites. It should be pointed out that the relative intensities of the saponite-related bands are lower than in the spectra of samples S, SC, and CS, due to the lower mass percentage of paraffin (67% w/w) in the composite than in bulk paraffin.

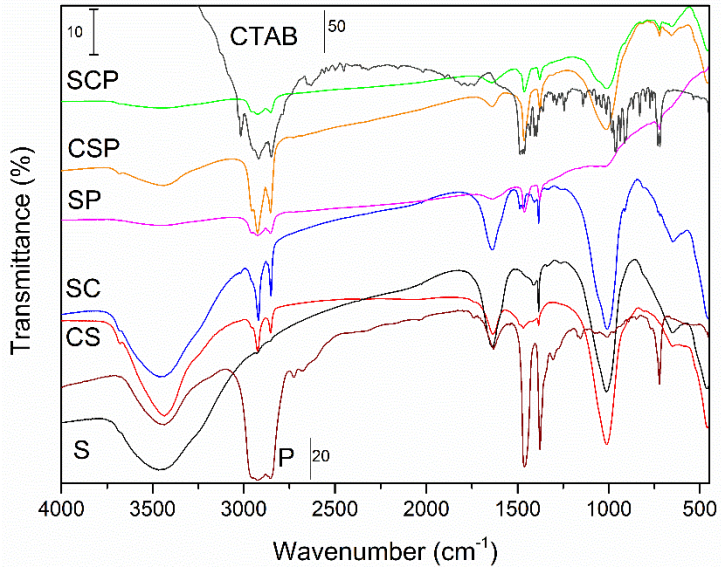

Figure 2. FT-IR spectra of the synthesized solids, and those of the paraffin (P) and CTAB as references.

The thermal curves (TG and DTA) of samples S, SC, CS and CTAB are shown in Figure 3. The DTA curve of sample S showed an endothermic effect from room temperature up to ca. 200 °C centred at 92 °C (as concluded from the DTG curve), which corresponds to a mass loss of 22% over the same temperature range in the TG curve, due to the removal of water. The TG curve showed a gentle decreasing slope between 200 and 700 °C due to the removal of interstitial water and the progressive dehydroxylation of the clay, but no relevant effects were observed in the DTA curve. In this temperature range, there was a total mass loss close to 5%. A mass loss corresponding to 2% of the initial sample mass was recorded between 700 and 800 °C, and this was associated with an endothermic effect centred at 776 °C caused by the removal of residual hydroxyl groups, resulting in a recrystallization which was responsible for the two exothermic effects recorded immediately afterwards, without any associated mass loss in the TG curve. The first peak, at 790 °C, is due to formation of enstatite and the segregation of silica [34], and the second one, at 833 °C, to the formation of mullite ($Al_6Si_2O_{13}$) [35]. The total mass loss was close to 28%.

The thermal analysis of pristine CTAB showed a weight loss of almost 100% of its initial weight from 25 to 500 °C. This suggests that the weight loss over this temperature range in samples SC and CS was mainly due to the decomposition of the surfactant in these samples. Over this range of temperatures, the slope of the TG curve of samples SC and CS decreased compared to that of the curve of CTAB; this indicates that the rate of the weight loss was a bit slower compared to pure CTAB when the surfactant was between the layers of the saponite. On the other hand, the decomposition pattern of pure CTAB displayed four well-differentiated exothermic effects in the DTA curve, while in those of SC and CS, only an exothermal effect could be perfectly differentiated—the other three were registered as shoulders.

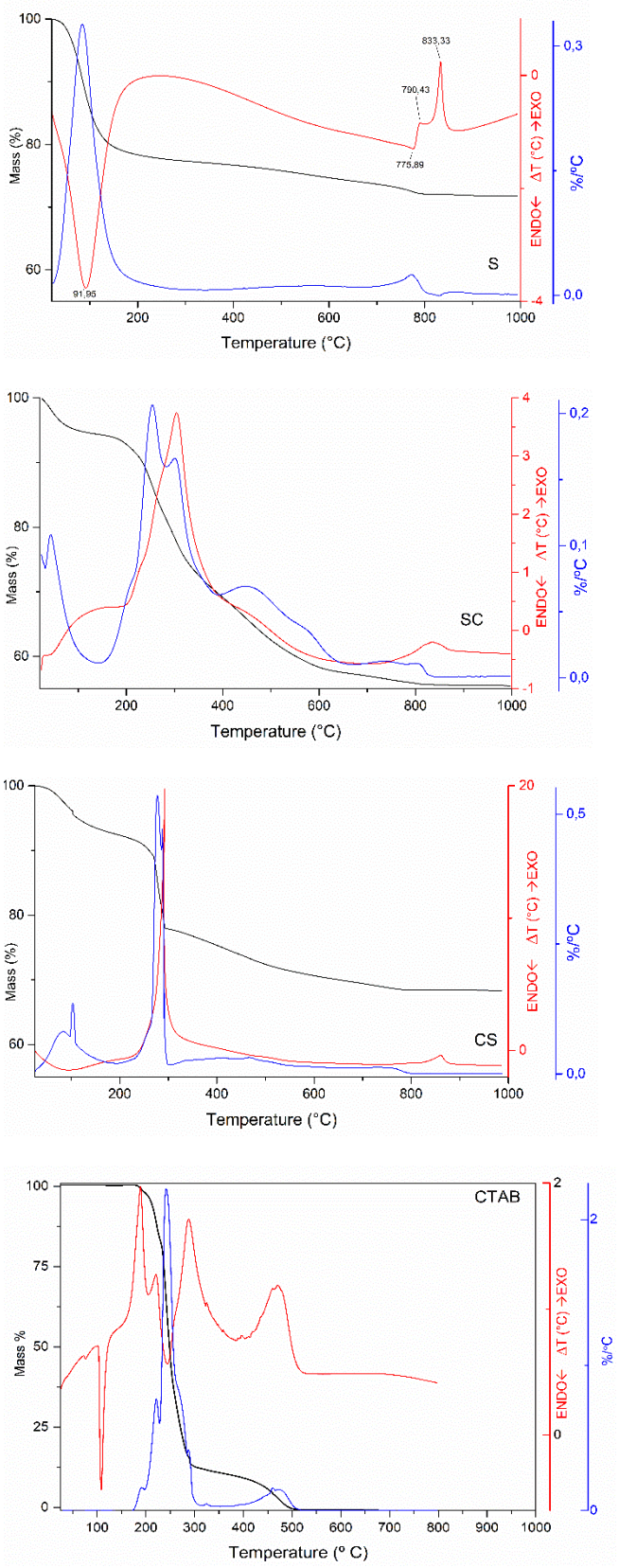

Figure 3. TG (black line) DTA (red line) and DTG (blue line) of samples S, SC, CS and CTAB.

The DTA curves for samples SC and CS, showed a primary weak endothermic effect from room temperature up to 200 °C due to water removal, with a corresponding mass loss of 7% in the TG curve. Between 200 and 600 °C, the DTA curves were dominated by

an intense exothermic effect (actually composed of four steps, according to the DTG curve) centred at 300 °C that could be ascribed to combustion of the hydrocarbon chain of the surfactant, with probable production of carbon dioxide and water vapor, as it coincided with the strong exothermic effect recorded for CTAB. This effect was followed by another that appeared as a shoulder at higher temperatures (around 400 °C) and was due to the total combustion of the surfactant. The thermal effects at higher temperatures (800–1000 °C) were not as well defined as for sample S. The shape of the first exothermic effect was broader and less intense for sample SC, thus indicating a lower ordering of the CTAB molecules in this sample. The total mass loss, higher for sample SC (around 42%) than for sample CS (30%), suggests a larger amount of surfactant adsorbed on the layers in sample SC. These results must be a consequence of differences in synthesis methods: the direct one-step synthesis method using microwave radiation gave rise to a better ordering of the CTAB molecules than in sample SC, synthesized by the conventional method.

The textural properties of the samples have been analysed by means of their N_2 adsorption–desorption isotherms (Figure 4). Table 1 shows the specific surface area values (SBET) calculated by the BET method [21], external surface (St), micropore volume and average pore diameter [22] for the synthesized saponites.

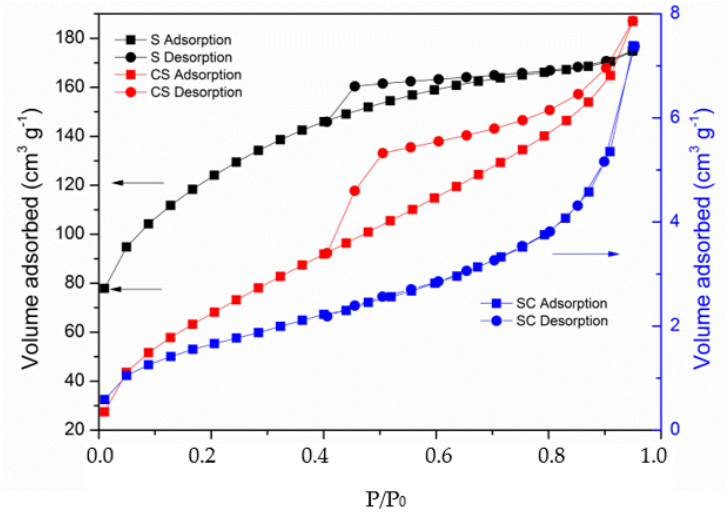

Figure 4. Nitrogen adsorption–desorption isotherms of samples S (black), SC (blue) and CS (red).

Table 1. Specific surface area (S_{BET}), external surface (S_t), micropore volume (V_{mp}) and average pore diameter (D_p) of samples S, SC and CS.

Sample	S_{BET} (m^2/g)	S_t (m^2/g)	V_{mp} (mm^3/g)	D_p (nm)
S	408	353	36	2.74
CS	252	252	-	4.14
SC	6	6	-	7.69

The shape of the adsorption isotherm for sample S (Figure 4) corresponded to Type I of the IUPAC classification, characteristic of solids with a small fraction of micropores, as confirmed by the sharp adsorption uptake at low relative pressures [23]. The external surface area, as determined by the t-method, was ca. 55 m^2/g lower than the BET value—this difference corresponding to the area equivalent to adsorption in micropores. The desorption branch showed a H2-type hysteresis loop, usually recorded in disordered materials whose shape and distribution of pores is not well defined—indicating the existence of inkbottle pores [23].

Sample SC showed completely reversible type II isotherm characteristics of a non-microporous solid, with a very limited adsorption capacity (see the different ordinate scale used in Figure 4 to plot this isotherm). The surface accessible to N_2 molecules in this

sample is almost cancelled, probably by the small particles of CTAB that block the entrance of N_2 into the pores. The isotherm for sample CS also corresponds to type II of the IUPAC classification, with a H2-type hysteresis loop that closes at a value of relative pressure close to 0.4. The larger S_{BET}, as compared to that of sample SC, is in agreement with the lower CTAB content of this sample. The S_{BET} and S_t values are coincident, suggesting the absence of micropores in this sample.

3.2. Thermal Properties of the Paraffin/Saponite Composites

3.2.1. DSC Analysis

The results obtained by DSC upon heating the PCMs are shown in Figure 5. The first peak corresponds to a solid–solid phase change (S-S) and the second one to a solid–liquid phase change (S-L) [7]. The temperatures of these effects for the three paraffin-containing samples are included in Table 2. The curve and the values for bulk paraffin (P) are given as well.

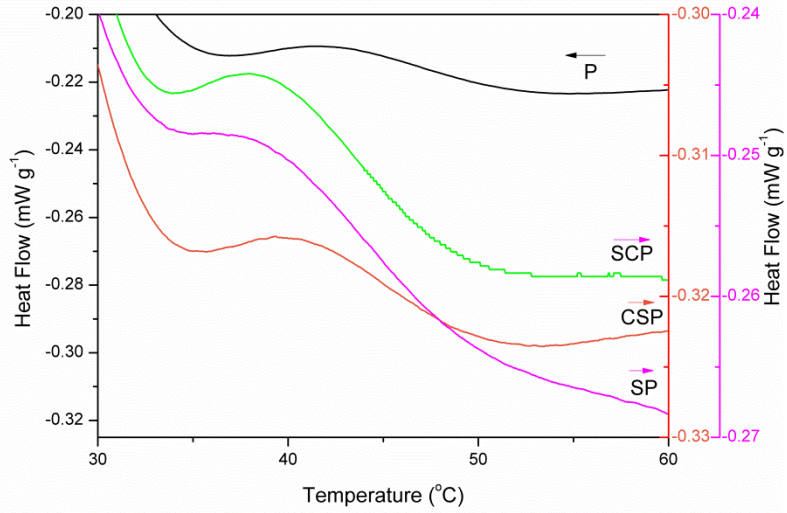

Figure 5. DSC curve of the paraffin/synthetic saponite PCMs and of bulk paraffin.

Table 2. Temperature (°C) of the effects recorded in the DSC.

	S-S	S-L
P	36.2	53.5
SP	32.8	50.0
SCP	33.2	49.5
CSP	34.2	50.5

The value of the phase change temperature depends on the interactions between the paraffin and the clay [24]; thus, strong interactions lead to an increase in the melting point, while weak interactions give rise to a decrease in the melting point [25]. The thermal characteristics of PCM were very close to those of paraffin (Figure 5), and in all cases, the heat flow was much lower for the samples synthetized here than for bulk paraffin (see the vertical scales in Figure 5). In other words, the presence of saponite in the composite leads to a small decrease (3.5–4 °C) in the melting point of paraffin. The values for the composites were very close to each other in all cases, and the decrease in the melting point of paraffin was small—probably because of the dispersion of the paraffin molecules on the clay surface.

3.2.2. Heat Storage and Heat Release Properties of Paraffin/Synthetic Saponite PCM

The heating and cooling curves of bulk paraffin, saponites and PCMs are included in Figure 6. As can be observed, the PCMs have in all cases a faster heating rate than paraffin,

suggesting the beneficial role of saponite in the composite, on compared with bulk paraffin. Regarding the release of heat (right hand side of Figure 6), the cooling rate was lower in the PCMs than in pure paraffin. Thus, it can be concluded that the synthetized composites store heat with much greater efficiency than paraffin, but they do not release it.

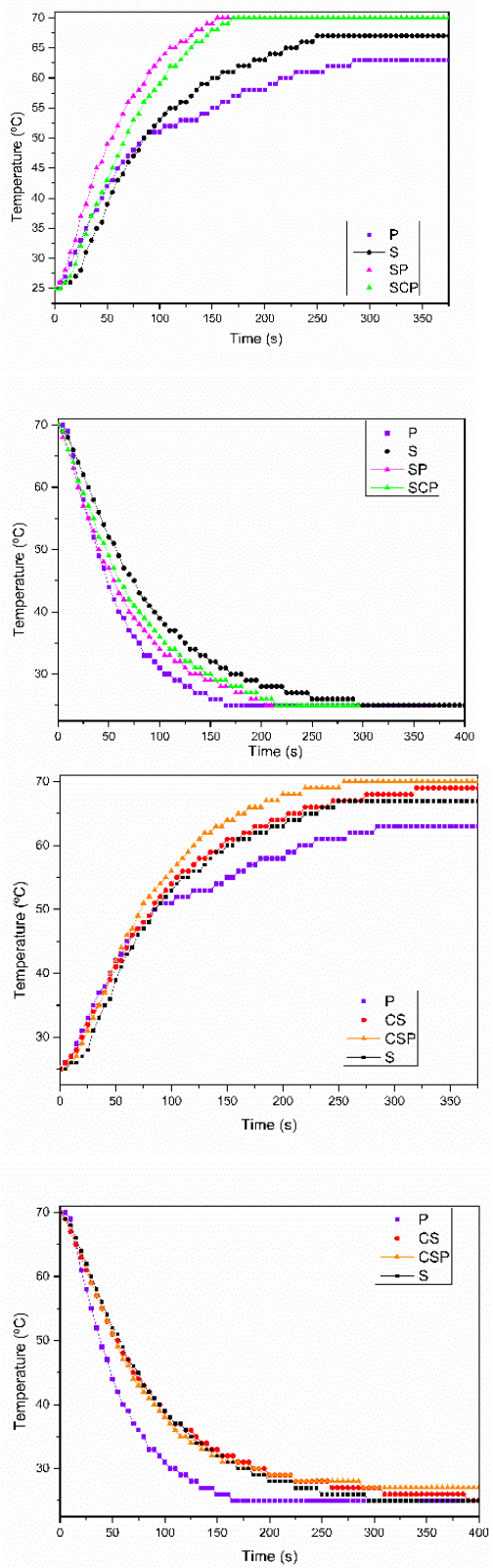

Figure 6. The heating (**top**) and cooling curves (**bottom**) of paraffin, saponite and PCMs. The curves for paraffin and saponite have been repeated for comparison purposes.

Bulk paraffin required 284 s to increase its temperature from room temperature (25 °C) to the maximum value of 60 °C. The time required to reach this temperature was 189 s for bulk saponite, 99 and 175 s for samples SP and CS, respectively, and, finally, 120 and 141 s for samples SCP and CSP, respectively. The maximum temperature attained by the composites was 70 °C.

On cooling from 70 °C to room temperature, the fastest response was shown by paraffin (165 s), while saponite (sample S) required 296 s. Concerning the treated saponites, the values were 205 and 391 for samples SP and CS, respectively, and 217 and >400 s for composites SCP and CSP, respectively. On comparing the behaviour shown by the composites, it can be concluded that the fastest heating was observed in sample SCP, while the slowest cooling was observed for sample CSP.

3.2.3. The Thermal Stability of the Paraffin/Synthetic Saponite PCM

One of the most relevant properties of PCMs is their responses upon several heating–cooling cycles. We have submitted the composites to ten heating–cooling cycles and the results for the first and the tenth ones are included in Figure 7. The phase change plateaux did not differ significantly after 10 cycles. This result indicates that the prepared paraffin/synthetic saponite PCMs can maintain their thermal properties even after ten cycles and display a good thermal stability. The only difference was found in the heating curve for sample CSP, as in the tenth cycle, the time required to reach the maximum temperature (70 °C) decreased from 255 to 154 s, improving the yield of this PCM even more.

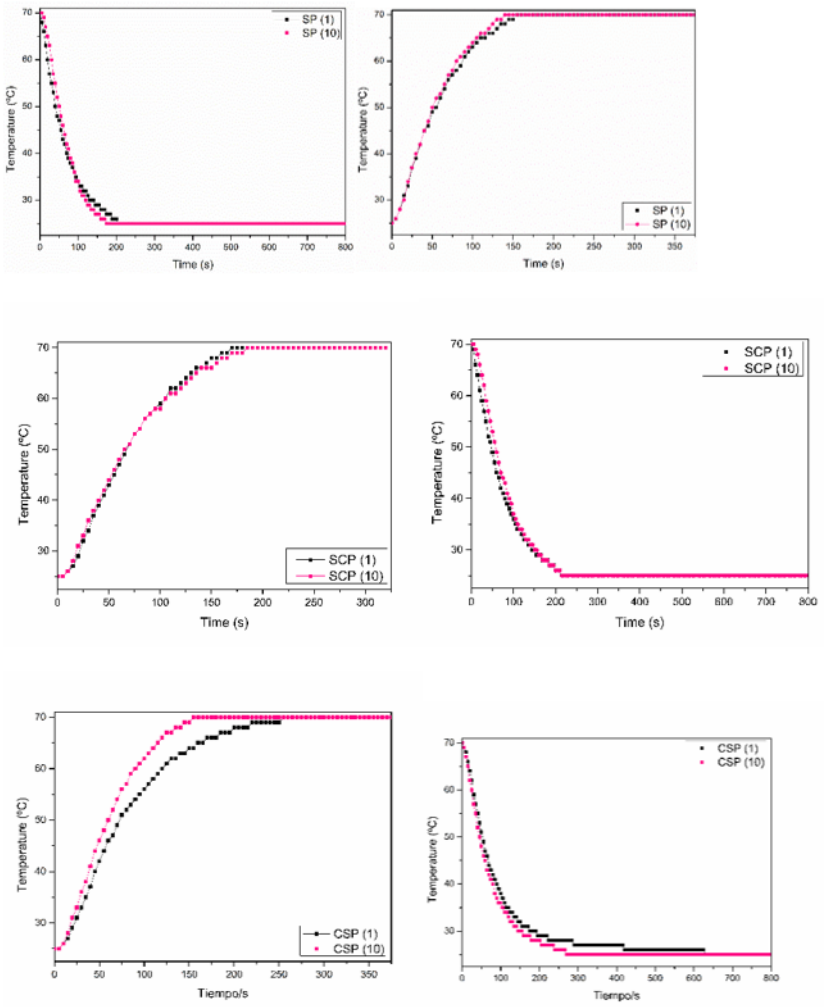

Figure 7. The heating curves (**left**) and cooling curves (**right**) of PCMs after 10 cycles.

4. Conclusions

Different PCMs based on synthetic saponite/paraffin were correctly prepared, as proven by characterization techniques such as FT-IR spectroscopy and powder X-ray diffraction. The prepared PCMs had a higher heating rate and a lower cooling rate than bulk paraffin because their heat storage was improved by the presence of synthetic saponites. These PCMs had good thermal properties and stability, so they could be tentatively applied in heat storage for energy saving in buildings. In view of the thermal properties and thermal stability study, the one-pot synthesised CSP seemed to be the most suitable for this use, as already mentioned. All the paraffin composites stored heat for almost 50% longer than paraffin; the CSP composite stored it for longer than all the others and, in addition, the time it took to reach the maximum temperature decreased as the heating–cooling cycles went on. Specifically, the time it took to reach this maximum fell to 60% by the tenth cycle. As such, this article has described a rapid and low-cost preparation method for an efficient PCM suitable for heat storage applications.

Author Contributions: Conceptualization, R.T. and V.R.; methodology, R.T. and V.R.; software, B.G.; validation, R.T., V.R. and B.G.; formal analysis, R.T. and V.R.; investigation, R.T., V.R. and B.G.; resources, V.R.; data curation, R.T. and V.R.; writing—original draft preparation, R.T. and B.G.; writing—review and editing, R.T. and V.R.; visualization, R.T., V.R. and B.G.; supervision, R.T. and V.R.; project administration, V.R.; funding acquisition, V.R. All authors have read and agreed to the published version of the manuscript.

Funding: This research received no external funding.

Conflicts of Interest: The authors declare no conflict of interest.

References

1. He, B.; Martin, V.; Setterwall, F. Phase transition temperature ranges and storage density of paraffin wax phase change materials. *Energy* **2004**, *29*, 1785–1804. [CrossRef]
2. Li, C.; Fu, L.; Ouyang, J.; Tang, A.; Yang, H. Kaolinite stabilized paraffin composite phase change materials for thermal energy storage. *Appl. Clay Sci.* **2015**, *115*, 212–220. [CrossRef]
3. Kang, P.; Liangjie, F.; Xiaoyu, L.; Jing, O.; Huaming, Y. Stearic acid modified montmorillonite as emerging microcapsules for thermal energy storage. *Applied. Clay Sci.* **2017**, *138*, 100–106.
4. Lv, P.; Liu, C.; Rao, Z. Review on clay mineral-based form-stable phase change materials: Preparation, characterization and applications. Renew. *Sustain. Energy Rev.* **2017**, *68*, 707–726. [CrossRef]
5. Sari, A. Thermal energy storage characteristics of bentonite-based composite PCMs with enhanced thermal conductivity as novel thermal storage building materials. *Energy Convers. Manag.* **2016**, *117*, 132–141. [CrossRef]
6. Sari, A. Thermal Energy Storage Properties and Laboratory-Scale Thermoregulation Performance of Bentonite/Paraffin Composite Phase Change Material for Energy-Efficient Buildings. *J. Mater. Civil Eng.* **2017**, *29*, 04017001. [CrossRef]
7. Obaje, S.O.; Omada, J.L.; Dambatta, U.A. Clays and their Industrial Applications: Synoptic Review. *Int. J. Sci. Technol.* **2013**, *3*, 264–270.
8. Ismadji, S.; Soetaredjo, F.E.; Ayucitra, A. *Clay Materials for Environmental Remediation*; Springer: Cham, Switzerland, 2015; pp. 1–124.
9. Okada, A.; Fukushima, Y.; Kawasumi, M.; Inagaki, S.; Usuki, A.; Sugiyama, S.; Kurauchi, T.; Kamigaito, O. Composite Material and Process for Manufacturing Same. U.S. Patent 4,739,007, 19 April 1988.
10. Kawasumi, M.; Kohzaki, M.; Kojima, Y.; Okada, A.; Kamigaito, O. Process for Producing Composite Material. U.S. Patent 4810734A, 7 March 1989.
11. Usuki, A.; Kojima, Y.; Kawasumi, M.; Okada, A.; Fukushima, Y.; Kurauchi, T.; Kamigaito, O. Synthesis of nylon 6-clay hybrid. *J. Mater. Res.* **1993**, *8*, 1179–1184. [CrossRef]
12. Kojima, Y.; Usuki, A.; Kawasumi, M.; Okada, A.; Fukushima, Y.; Kurauchi, T.; Kamigaito, O. Mechanical properties of nylon 6-clay hybrid. *J. Mater. Res.* **1993**, *8*, 1185–1189. [CrossRef]
13. Sarier, N.; Onder, E.; Ozay, S.; Ozkilic, Y. Preparation of phase change material–montmorillonite composites suitable for thermal energy storage. *Thermochim. Acta* **2011**, *524*, 39–46. [CrossRef]
14. Lim, S.C.; Gomes, C.; Kadir, M.Z.A.A. Preliminary grounding performance of bentonite mixed concrete encased steel cage under high soil resistivity condition. *Int. J. Elec. Power* **2013**, *47*, 117–128. [CrossRef]
15. Sarı, A. Fabrication and thermal characterization of kaolin-based composite phase change materials for latent heat storage in buildings. *Energy Build.* **2015**, *96*, 193–200. [CrossRef]

16. Yang, D.; Peng, F.; Zhang, H.; Guo, H.; Xiong, L.; Wang, C.; Shi, S.; Chen, X. Preparation of palygorskite paraffin nanocomposite suitable for thermal energy storage. *Appl. Clay Sci.* **2016**, *126*, 190–196. [CrossRef]
17. Farid, M.M.; Khudhair, A.M.; Ali, S.; Razack, K.; Al-Hallaj, S. A review on phase change energy storage: Materials and applications. *Energy Convers. Manag.* **2004**, *45*, 1597–1615. [CrossRef]
18. Cárdenas-Ramírez, C.; Jaramillo, F.; Gómez, M. Systematic review of encapsulation and shape-stabilization of phase change materials. *J. Energy Storage* **2020**, *30*, 101495. [CrossRef]
19. Umair, M.M.; Zhang, Y.; Iqbal, K.; Zhang, S.; Tang, B. Novel strategies and supporting materials applied to shape-stabilize organic phase change materials for thermal energy storage—A review. *Appl. Energy* **2019**, *235*, 846–873. [CrossRef]
20. Rathore, P.K.S.; Shukla, S.K. Enhanced thermophysical properties of organic PCM through shape stabilization for thermal energy storage in buildings: A state of the art review. *Energy Build.* **2021**, *236*, 110799. [CrossRef]
21. Li, M.; Wu, Z.; Kao, H.; Tan, J. Experimental investigation of preparation and thermal performances of paraffin/bentonite composite phase change material. *Energy Convers. Manag.* **2011**, *52*, 3275–3281. [CrossRef]
22. Gao, F. Clay/polymer composites: The story. *Mater. Today* **2004**, *7*, 50–55. [CrossRef]
23. Trujillano, R.; Rico, E.; Vicente, M.A.; Rives, V.; Bergaoui, L.; Chaabene, S.B.; Ghorbel, A. Microwave-Assisted Synthesis of Fe^{3+} Saponites. Characterization by X-Ray Diffraction and FT-IR Spectroscopy. *Macla* **2009**, *11*, 189–190.
24. Brunauer, S.; Emmett, P.H.; Teller, E. Absorption of Gases in Multimolecular Layers. *J. Am. Chem. Soc.* **1938**, *60*, 309–319. [CrossRef]
25. Barrett, E.P.; Joyner, L.G.; Halenda, P.P. The Determination of Pore Volume and Area Distributions in Porous Substances. I. Computations from Nitrogen Isotherms. *J. Am. Chem. Soc.* **1951**, *73*, 373–380. [CrossRef]
26. Lowell, S.; Shields, J.; Thomas, M.A.; Thommes, M. *Characterization of Porous Solids and Powders: Surface Area, Pore Size and Density*; Springer: Dordrecht, The Netherlands, 2010; pp. 1–338.
27. Li, M.; Guo, Q. The preparation of the hydrotalcite-based composite phase change material. *Appl. Energy* **2015**, *156*, 207–212. [CrossRef]
28. Suquet, H.; de la Calle, C.; Pezerat, H. Swelling and structural organization of saponite. *Clays Clay Min.* **1975**, *23*, 1–9. [CrossRef]
29. Trujillano, R.; Rico, E.; Vicente, M.A.; Herrero, M.; Rives, V. Microwave radiation and mechanical grinding as new ways for preparation of saponite-like materials. *Appl. Clay Sci.* **2010**, *48*, 32–38. [CrossRef]
30. Ahlrichs, J.L.; Serna, C.; Serratosa, J.M. Structural hydroxyls in sepiolites. *Clays Clay Min.* **1975**, *23*, 119–124. [CrossRef]
31. Madejová, J. FTIR techniques in clay mineral studies. *Vibr. Spect.* **2003**, *31*, 1–10. [CrossRef]
32. Su, G.; Yang, C.; Zhu, J.J. Fabrication of Gold Nanorods with Tunable Longitudinal Surface Plasmon Resonance Peaks by Reductive Dopamine. *Langmuir* **2015**, *31*, 817–823. [CrossRef]
33. Cho, S.Y.; Fogle, H.S. Efforts on solving the problem of paraffin deposit. I: Using oil-soluble inhibitors. *J. Ind. Eng. Chem.* **1999**, *5*, 123–127.
34. MacKenzie, R.C. Simple phyllosilicates based on gibbsite- and brucite-like sheets. In *Differential Thermal Analysis*; Academic Press: London, UK, 1973; Volume 1, pp. 498–538.
35. Vicente, M.A.; Lambert, J.-F. Synthesis of Pt pillared clay nanocomposite catalysts from $[Pt^{II}(NH_3)_4]Cl_2$ precursor. *Phys. Chem. Chem. Phys.* **2001**, *3*, 4843–4852. [CrossRef]